



Aalborg Universitet

AALBORG UNIVERSITY  
DENMARK

## Flexible power control strategy for elliptical trajectory based dynamic voltage restorer during voltage sags

Li, Peng; Wang, Yi; Wang, Can; Pan, Xuwei; Lu, Jinghang; Li, Xue; Blaabjerg, Frede

*Published in:*  
IET Renewable Power Generation

*DOI (link to publication from Publisher):*  
[10.1049/rpg2.12222](https://doi.org/10.1049/rpg2.12222)

*Creative Commons License*  
CC BY 4.0

*Publication date:*  
2021

*Document Version*  
Publisher's PDF, also known as Version of record

[Link to publication from Aalborg University](#)

*Citation for published version (APA):*

Li, P., Wang, Y., Wang, C., Pan, X., Lu, J., Li, X., & Blaabjerg, F. (2021). Flexible power control strategy for elliptical trajectory based dynamic voltage restorer during voltage sags. *IET Renewable Power Generation*, 15(13), 2904-2917. <https://doi.org/10.1049/rpg2.12222>

### General rights


Copyright and moral rights for the publications made accessible in the public portal are retained by the authors and/or other copyright owners and it is a condition of accessing publications that users recognise and abide by the legal requirements associated with these rights.

- Users may download and print one copy of any publication from the public portal for the purpose of private study or research.
- You may not further distribute the material or use it for any profit-making activity or commercial gain
- You may freely distribute the URL identifying the publication in the public portal -

### Take down policy

If you believe that this document breaches copyright please contact us at [vbn@aub.aau.dk](mailto:vbn@aub.aau.dk) providing details, and we will remove access to the work immediately and investigate your claim.

# Flexible power control strategy for elliptical trajectory based dynamic voltage restorer during voltage sags

Peng Li<sup>1</sup> | Yi Wang<sup>1</sup> | Can Wang<sup>1</sup> | Xuewei Pan<sup>1</sup> | Jinghang Lu<sup>1</sup> | Xue Li<sup>2</sup> |  
Frede Blaabjerg<sup>3</sup> 

<sup>1</sup> School of Mechanical Engineering and Automation, Harbin Institute of Technology, HIT Campus of University Town of Shenzhen, China

<sup>2</sup> North China University of Water Resources and Electric Power, Zhengzhou, China

<sup>3</sup> Department of Energy Technology, Aalborg University, Aalborg, Denmark

## Correspondence

Can Wang, School of Mechanical Engineering and Automation, Harbin Institute of Technology, HIT Campus of University Town of Shenzhen, China.  
Email: can.wang@hit.edu.cn

## Funding information

China Postdoctoral Science Foundation, Grant/Award Number: 2020M681093; Shenzhen Basic Research, Grant/Award Number: JCYJ20180306172056738

## Abstract

Dynamic voltage restorer (DVR) plays an essential role in achieving high-quality voltage restoration in the distribution system. This paper presents an elliptical-trajectory-based approach to guarantee continuous power delivery by considering the active and reactive power limits during voltage sags. Besides, two parameters are proposed in the accurate mathematical analysis of current references. Thus, the control objective can be fulfilled by the flexible current injection strategy that combines a precise balance between the positive and negative sequences. The proposed control method can determine the required power injections by selecting the two proper values to support that the converter output current is smaller than the maximum rated value. Under the presented control, the maximum power limit and flexible power dispatch are combined together to develop four operation schemes. The main advantage is the smooth transition process during changes in the operation schemes and the disappearance of active and reactive power oscillations. Also, these four control states are applied to reveal the flexibility of the proposed designs. Finally, the hardware tests in a laboratory prototype are implemented to validate the feasibility of the proposed method.

## 1 | INTRODUCTION

Nowadays, the traditional configuration of the electrical AC network is changing, and the high penetration of grid-connected distributed generation (DG) sources located at the point of power consumption is increasing significantly due to the elimination of local restrictions in the electric power distribution [1, 2]. Thence, there is a negative influence on the total reliability of the grid infrastructure because of the greater integration of DG techniques [3]. One of the most challenging disturbances is known as voltage sag, which reflects a sharp reduction of the voltage amplitude and the fluctuation of the phase jump in one or more grid phases [4, 5]. Thus, the mitigation of voltage sags is the chief candidate to offer better system stability, which is also the most attractive solution to voltage quality improvement. At present, dynamic voltage restorer (DVR) is accepted as a reliable solution to remove the voltage sag from the substations and feeders [6, 7]. Mainly, the DVR cannot only perform the gen-

eral manner of voltage restoration, but it can maintain the safe operation condition for sensitive load without obtrusive interruption.

At the same time, the current trend developing the voltage restoration criteria for DVR based on the instantaneous power theory has emerged in [8–11]. An existing approach to deal with any kind of voltage sag can be used to eliminate the phase jumps at the expense of considerable active power demands, which is defined as pre-phase compensation [8]. Other solutions, including in-phase strategy [9] or energy-optimized strategy [10, 11], have been proposed to reduce storage energy up to its lowest capacity, in which it is difficult to compensate for the phase jump.

Moreover, the idea of elliptical trajectory compensation with optimal volt-ampere (VA) sizing is presented in [12, 13].

Nevertheless, the individual control of active and reactive power delivery has not been studied. From the power source's point of view, the actual DVR capacity is limited by the

This is an open access article under the terms of the [Creative Commons Attribution](https://creativecommons.org/licenses/by/4.0/) License, which permits use, distribution and reproduction in any medium, provided the original work is properly cited.

© 2021 The Authors. *IET Renewable Power Generation* published by John Wiley & Sons Ltd on behalf of The Institution of Engineering and Technology

maximum amplitude of the power converter current. Meanwhile, the DVR should be able to overcome the large currents caused by temporary voltage sag and continue to maintain the load stability. Thus, in order to satisfy these requirements, some specific control schemes have to be introduced to accomplish continuous power delivery within the limit of power capacity required by the loads, thus ensuring that the maximum current of voltage source converters (VSCs) is restrained to the normal rated value [14, 15].

Next, most of the works are based on symmetric sequences [16, 17] to develop the different control structures and guarantee the flexible power provisions once the voltage sag occurs. Some of the control strategies provide adjustable power delivery under voltage sags [18, 19]. Still, the mentioned studies fail to reach an agreement with the peak power limitation that is used to maintain the injected power within the upper boundary, especially for the use of DVR. Thus, a modified algorithm based on the elliptical trajectory is proposed when taking into account the adjustable power delivery. Also, the proposed method in this paper can be realized by the selection of the two control parameters, thus guaranteeing the power dispatch within the power limits during voltage sags. In other words, the maximum power limit and flexible power delivery are combined together by selecting the proper values of two parameters so that it gives priority to either active power injection or reactive power injection as established by the load demands. Then, one set of reference generators that provides proposed power injection characteristics will be discussed depending on two main aspects [20–22]. Firstly, two individual parameters established by the reference operators can offer maximum active (or reactive) power. For example, the mentioned maximum value of reactive power is determined to guarantee that the maximum current of the voltage source converter is not exceeded during voltage sags. And secondly, the power dispatch strategy can be achieved to accomplish the continuous power delivery by considering two maximum power values during voltage sags [23, 24].

Thus, the objective of this paper is to propose an elliptical-trajectory-based design of power restriction for DVR. The contributions of this paper are: 1) A new mechanism of power control incorporating critical parameters  $k_p$ ,  $k_q$  are proposed to achieve flexible power dispatch of DVR. The  $k_p$ ,  $k_q$  can be adjusted according to the need of the load while keeping the load voltage within a safe range. The control approach can calculate the current references by selecting the two individual parameters  $k_p$ ,  $k_q$  to accomplish different power injection. Four situations are demonstrated to choose the parameter values. The active and reactive power injection characteristics can be tuned to fulfill adjustable power dispatch needed by the specific loads. 2) In addition to adjustable control of DVR output power, the mitigation of power oscillation, the smooth transition process of power control, and optimized power capacity are realized simultaneously by means of the voltage sag compensation of the elliptical trajectory. 3) A new protection mechanism based on the power delivery limits is also designed.

This paper is organized as follows. A brief survey of the elliptical trajectory and the entire mathematical investigation and the

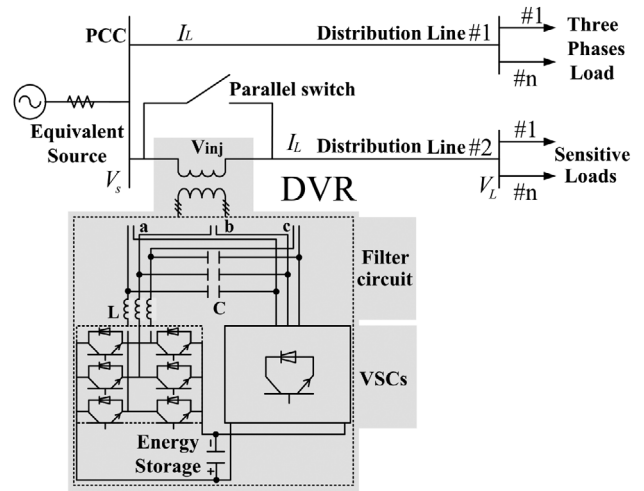


FIGURE 1 System configuration of the DVR unit

new forms of adjustable current references are given in Section 2. Section 3 provides the description of the proposed control algorithm to determine maximum power restrictions and presents the flexible power dispatch. The lab tests to illustrate the advantage of the proposed method are added in Section 4. Section 5 presents the conclusion of this paper.

## 2 | SYSTEM DESCRIPTION AND VOLTAGE SAG CHARACTERIZATION

In order to facilitate the following analysis, the particular vector relationships in the AC grid will be defined in a per-unit (p.u.) system. Besides, the harmonic distortion has not been taken into consideration during voltage sags in this paper. Figure 1 shows the typical configuration of a DVR [13]. The complete system is composed of the AC grid (i.e. equivalent source), the DVR unit and the sensitive loads. The DVR unit is connected to the distribution line through the second winding of the injection transformer. Two parallel-connected pulsewidth-modulation (PWM) converters are connected to the primary of the injection transformer through the  $LC$  filter, and a dc-side unit is utilized as an energy storage. Figure 2 shows a typical vector diagram for the compensation algorithm of the elliptical trajectory, as also discussed in [13]. A chief feature of the control strategy is to guarantee that any voltage perturbation can be compensated, and the load voltage, therefore, fails to be afflicted. The main targets shown in Figure 2 are to provide the output voltage of  $\vec{V}_{inj}$  based on the elliptical restoration criteria [12]. The detailed descriptions for this output voltage can be expressed by the specific ellipse parameters. For instance, the geometrical relationship of an ellipse centered at point  $O$  can be realized, in which major axis is  $V_x$  and  $V_r$  is the minor axis.

The vectors  $\vec{V}_L$  and  $\vec{I}_L$  denote load voltage and current, respectively, and the corresponding magnitude is depicted by a capital letter without any overhead sign. To emphasize the differences with the method in [13], the magnitudes of load voltage



**Function:**  $(\vec{i}_p^*, \vec{i}_q^*) = \text{Control Support}(\vec{V}_\alpha^\pm, \vec{V}_\beta^\pm, P_{dc})$

---

- 1 obtain  $\vec{V}_\alpha^\pm, \vec{V}_\beta^\pm, P_{dc}$  / \* Raw Signals \*/
- 2 set  $I_N$  & calculate  $P_{max}$  (22) / \* Pre-Process \*/
- 3 if  $P_{dc} > P_{max}$  / \* Classification \*/
- 4 then set  $P^* = P_{max}$  &  $Q^* = 0$  / \* Feature Selection \*/
- 5 else set  $P^* = P_{dc}$  &  $Q^* = Q_N$  / \* Feature Selection \*/
- 6 return  $(\vec{i}_p^*, \vec{i}_q^*)$

---

**FIGURE 3** Pseudocode for the controller implementation of the proposed control strategy

$$\vec{i}_q^+ = \vec{i}_{\alpha(q+)}^+ + \vec{i}_{\beta(q+)}^+ = -\frac{-k_q^+ Q(-\vec{V}_\alpha^+ + \vec{V}_\beta^+)}{k_p^+ (V^+)^2 + k_q^+ (V^-)^2}, \quad (10)$$

$$\vec{i}_p^- = \vec{i}_{\alpha(p-)}^- + \vec{i}_{\beta(p-)}^- = \frac{k_p^- P(\vec{V}_\alpha^- + \vec{V}_\beta^-)}{-k_p^- (V^+)^2 + k_q^- (V^-)^2}, \quad (11)$$

$$\vec{i}_q^- = \vec{i}_{\alpha(q-)}^- + \vec{i}_{\beta(q-)}^- = -\frac{-k_q^- Q(-\vec{V}_\alpha^- + \vec{V}_\beta^-)}{-k_p^- (V^+)^2 + k_q^- (V^-)^2}, \quad (12)$$

where  $k_p^+$ ,  $k_p^-$ ,  $k_q^+$  and  $k_q^-$  are the control parameters. These parameters can be changed from 0 and 1. Thus, based on (9)–(12), the proposed algorithm of the reference generators is presented to display a prominent characteristic in Figure 3. Obviously, the preliminary processing performs a series of mathematical calculations from the sequence extractor ( $\vec{V}_\alpha^\pm, \vec{V}_\beta^\pm$ ), or the regulatory operation of dc-side voltage controller ( $P_{dc}$ ). Besides, using the defined two conditions of both  $P_{max}$  (22) and  $I_{max} = I_N$  as well as  $Q^* = 0$ , the setting process and the principle of self-determination can be achieved in the first two steps. Then, the key action is the feature selection that can decide the switching action (i.e. control condition). When the comparison result of two parameters (i.e.  $P_{dc}$  and  $P_{max}$ ) satisfies the classification rule, one strategy of power restriction will be activated. As a result, the active power must be designed as  $P^* = P_{max}$ , and the reactive power has to keep the minimum value ( $Q^* = 0$ ). On the other hand, if the proposed comparison result can not satisfy the classification rule, another strategy of active power is activated. Thence, a substantial quantity of the reactive power needs to be calculated as  $Q^* = Q_N = I_q^* ((\vec{V}_\alpha^+)^2 + (\vec{V}_\beta^+)^2)^{0.5}$ , and the required active power has to satisfy the condition ( $P^* = P_{dc}$ ). The last step involves the internal formations of the algorithm that determines the current references using the corresponding two power values.

### 3 | THEORETICAL APPROACH TO THE CONTROL STRATEGY

In order to preserve the controllability, two joint strategies are proposed to simplify (9)–(12) by linking the two control param-

eters. To differ from the pair symbols  $k_p^+$  and  $k_p^-$  or  $k_q^+$  and  $k_q^-$ , the parameter related to active and reactive power in the following is designed with  $k_p$  or  $k_q$ , respectively.

- 1) Joint strategy with opposing-sign coefficients  
Since the  $\alpha\beta$  frame is used, it can be derived that

$$\begin{bmatrix} i_\alpha^+ \\ i_\beta^+ \end{bmatrix} = \frac{1}{\sqrt{(\vec{V}_\alpha^+)^2 + (\vec{V}_\beta^+)^2}} \begin{bmatrix} \vec{V}_\alpha^+ & -\vec{V}_\beta^+ \\ \vec{V}_\beta^+ & \vec{V}_\alpha^+ \end{bmatrix} \begin{bmatrix} i_p^+ \\ i_q^+ \end{bmatrix}. \quad (13)$$

By defining  $k_p = k_p^+ = -k_p^-$  in (9) and (11), the resulting currents in the  $\alpha\beta$  frame can be adjusted by  $k_p$ . Then, using (1), (9) and (11), a new set of active current references can be easily calculated by applying the inverse-transformation for three-phase stationary reference frame (SRF) currents.

- 2) Joint strategy with same-sign coefficients

Similar to (13), it can also be derived that

$$\begin{bmatrix} i_\alpha^- \\ i_\beta^- \end{bmatrix} = \frac{1}{\sqrt{(\vec{V}_\alpha^-)^2 + (\vec{V}_\beta^-)^2}} \begin{bmatrix} \vec{V}_\alpha^- & -\vec{V}_\beta^- \\ \vec{V}_\beta^- & \vec{V}_\alpha^- \end{bmatrix} \begin{bmatrix} i_p^- \\ i_q^- \end{bmatrix}. \quad (14)$$

Again, by defining  $k_q = k_q^+ = k_q^-$  in (10) and (12), the resulting currents can also be adjusted by  $k_q$ . Then, using (1), (10) and (12), a new set of reactive current references can also be easily computed by applying the inverse-transformation for three-phase SRF currents.

Furthermore, the positive and negative current in (13) and (14) are

$$\begin{aligned} i_\alpha^+ &= \vec{i}_{\alpha(p+)}^+ + \vec{i}_{\alpha(q+)}^+, & i_\beta^+ &= \vec{i}_{\beta(p+)}^+ + \vec{i}_{\beta(q+)}^+, \\ i_\alpha^- &= \vec{i}_{\alpha(p-)}^- + \vec{i}_{\alpha(q-)}^-, & i_\beta^- &= \vec{i}_{\beta(p-)}^- + \vec{i}_{\beta(q-)}^-. \end{aligned} \quad (15)$$

A more detailed analysis reveals that the merging strategies (1) and (2) can be put together, and the proposed reference current are simplified as follows:

$$\vec{i}_{\alpha(p)}^* = \vec{i}_{\alpha(p+)}^* + \vec{i}_{\alpha(p-)}^* = \frac{k_p P^* (\vec{V}_\alpha^+ - \vec{V}_\alpha^-)}{k_p (V^+)^2 + k_q (V^-)^2}, \quad (16)$$

$$\vec{i}_{\beta(p)}^* = \vec{i}_{\beta(p+)}^* + \vec{i}_{\beta(p-)}^* = \frac{k_p P^* (\vec{V}_\beta^+ - \vec{V}_\beta^-)}{k_p (V^+)^2 + k_q (V^-)^2}, \quad (17)$$

$$\vec{i}_{\alpha(q)}^* = \vec{i}_{\alpha(q+)}^* + \vec{i}_{\alpha(q-)}^* = \frac{-k_q Q^* (\vec{V}_\beta^+ + \vec{V}_\beta^-)}{k_p (V^+)^2 + k_q (V^-)^2}, \quad (18)$$

$$\vec{i}_{\beta(q)}^* = \vec{i}_{\beta(q+)}^* + \vec{i}_{\beta(q-)}^* = \frac{k_q Q^* (\vec{V}_\alpha^+ + \vec{V}_\alpha^-)}{k_p (V^+)^2 + k_q (V^-)^2}. \quad (19)$$

From (16) to (19), the output current amplitudes depending on the two parameters, sag properties, and the reference powers can be achieved. These amplitudes are calculated by applying the inverse Clark transformation as follows:

$$I_x = \Delta I \sqrt{(V^+)^2 + (V^-)^2 - 2V^+V^- \cos_x}, \quad (20)$$

where  $x = a, b, \text{ or } c$ ,

$$\Delta I = \sqrt{\left(\frac{k_p P^*}{k_p (V^+)^2 + k_q (V^-)^2}\right)^2 + \left(\frac{k_q Q^*}{k_p (V^+)^2 + k_q (V^-)^2}\right)^2}.$$

The function  $\cos_x$  can be given as  $\cos_x(\varphi^+ - \varphi^- + m\frac{2\pi}{3})$ , where  $m = 0, 1, \text{ or } 2$ . Then, the maximum amplitude of phase current can be satisfied as follows:

$$I_{\max} = \Delta I \sqrt{(V^+)^2 + (V^-)^2 - 2V^+V^- \cos_{\min}}, \quad (21)$$

where  $\cos_{\min} = \text{Min}\{\cos_x\}$ .

To avoid converter damage and disconnection by the over-current,  $I_{\max}$  must be limited to the VSC-maximum-rated current by means of the designed condition:  $0 \leq I_{\max} \leq I_N$ .

### 3.1 | Determining maximum active and reactive power

The maximum amount of output powers during voltage sags should be determined based on  $I_{\max}$ . One depth analysis of (20) and (21) indicates that there exists a separate solution for  $P$  or  $Q$  in each expression. For instance, if the load current is larger than the certain threshold (i.e.  $I_N$ ), a reduction mechanism for a high level of redundancy among active power is also needed. Then, there exists a solution labeled  $P^* = P_{\max}$  in (21), which must comply with  $I_{\max} = I_N$  and  $Q^* = 0$ , and the final solution to the maximum active power is given as follows:

$$P_{\max} = \frac{I_{\max} U}{\sqrt{U - 2V^+V^- \cos_{\min}}}, \quad (22)$$

where  $U = (k_p (V^+)^2 + k_q (V^-)^2)$ .

On the other hand, if the load current is smaller than the maximum value, and then, one amplification mechanism for the supplementary reactive power is also required to maintain the load current at the normal rated level. Under this situation, by utilizing  $I_{\max} = I_N$  and  $P^* = P_{dc}$ , the solution in (21) for the reactive power, which ensures the maximum current limitation, is given as follows

$$Q_{inj}^* = U \sqrt{\frac{I_N^2}{U - 2V^+V^- \cos_{\min}} - \left(\frac{P_{dc}}{U}\right)^2}. \quad (23)$$

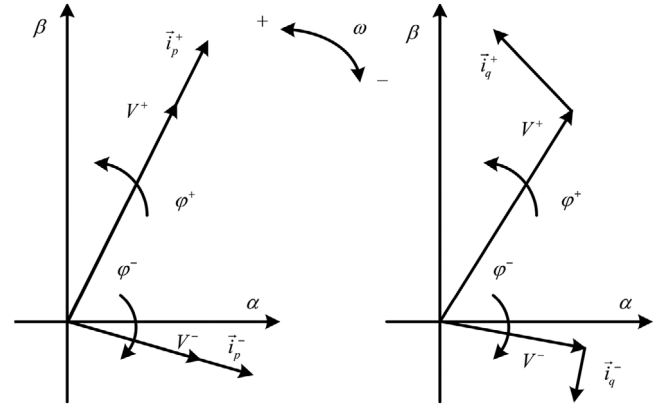


FIGURE 4 Vector diagram of the rms strategy. (Left) Maximum active power; (Right) maximum reactive power

Again, the maximum output reactive power is can also calculated from (21) utilizing the condition of  $I_{\max} = I_N$  and  $P^* = 0$ .

$$Q_{\max} = \frac{I_{\max} U}{\sqrt{U - 2V^+V^- \cos_{\min}}}. \quad (24)$$

Similar to (23), if the load current is less than the maximum value, again, and another amplification mechanism for the additional active power is also needed to hold the highest amounts of load current. Under this condition, by using  $I_{\max} = I_N$  and  $Q^* = Q_N = I_q^* ((\vec{V}_\alpha^+)^2 + (\vec{V}_\beta^+)^2)^{0.5}$ , the solution in (21) for the reference active power, which ensures the maximum rated current limitation, is calculated

$$P_{inj}^* = U \sqrt{\frac{I_N^2}{U - 2V^+V^- \cos_{\min}} - \left(\frac{Q_N}{U}\right)^2}. \quad (25)$$

Figure 4 displays the vector diagram in these two extreme conditions in (22) and (24): turning the active and reactive powers up to the maximum values, respectively.

Thus, the mentioned control strategy that determines adequate the power references ( $P^*$ ,  $Q^*$ ) to fulfill the proposed control objectives is presented. The operation of the protection mechanism can be described by the flowchart shown in Figure 5. Obviously, the raw signals (e.g.  $\vec{V}_\alpha^\pm$ ,  $\vec{V}_\beta^\pm$ ) from the sequence extractor and the regulatory operation of dc-side voltage controller (e.g.  $P_{dc}$ ) can be obtained from the Figure 3. Next, the maximum allowable active and reactive powers ( $P_{\max}$ ,  $Q_{\max}$ ) are calculated considering the value of the maximum current that the VSC can provide ( $I_{\max}$ ). Afterward, the rated load current  $I_N$  is compared with  $I_{\max}$  to determinate the protection mechanism. If this comparison result satisfies the classification rule, the suitable control action (i.e. protection mechanism) is activated. Thus, the key action is the feature selection that can decide two set of parameters ( $P^* = P_{\max}$ ,  $Q^* = Q_{inj}^*$  or  $P^* = P_{inj}^*$ ,  $Q^* = Q_{\max}$ ). On the other hand, if  $I_{\max}$  is lower than  $I_N$ , another strategy of active power will be activated. Thence, a

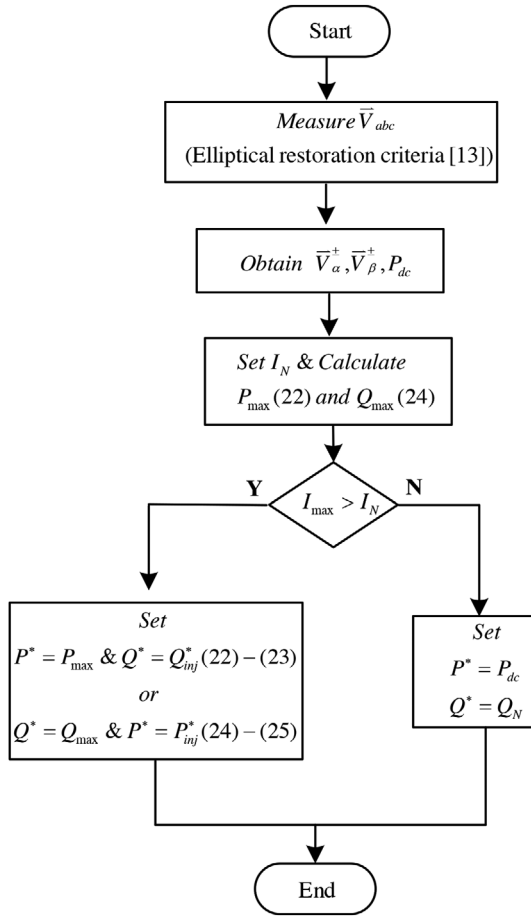


**FIGURE 5** Flow chart of the algorithm, which determines the protection mechanism under different voltage sags

substantial quantity of the reactive power  $Q^*$  needs to be calculated and the required active power has to satisfy the condition ( $P^* = P_{dc}$ ). Finally, the internal formations of the algorithm that determines the current references can be achieved.

### 3.2 | Proposed control scheme

According to the above discussions, this subsection provides four control situations (CS), under which the proposed control scheme is able to deal with. The first control situation noted as CS1 is created for the normal operation voltage range at the point of common coupling (PCC). The same reason also holds for the last three control situations marked as CS2, CS3, and CS4, respectively. The selection of two parameters is discussed under these four situations, and the major objective of the proposed control scheme is to realize the flexible active and reactive power dispatches.

The block diagram of the proposed compensation algorithm is shown in Figure 6. The inputs of the controller include the measured PCC voltages, the load currents, and the dc-side voltage. Firstly, the measured PCC voltages are processed on the basis of the elliptical trajectory theory. The instantaneous values are obtained in the  $\alpha\beta$  frame by using Clarke

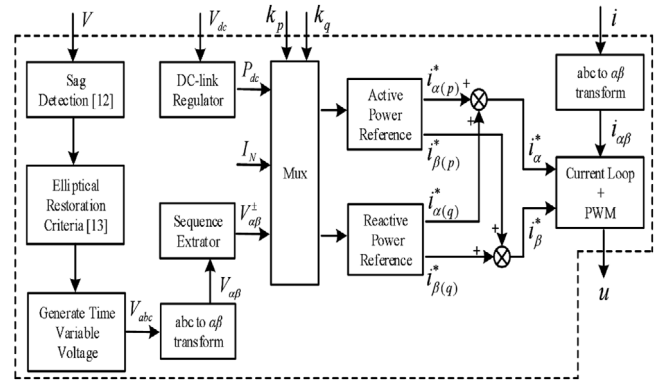


**FIGURE 6** The block diagram of the proposed compensation algorithm

transformation, and thus the corresponding SRF values can be decomposed into symmetric components (i.e.  $V_{\alpha\beta}^\pm$ ) using a sequence extractor. Then, the Mux block is responsible for estimating the current references while taking into account of the active and reactive power references ( $P^* = P_{dc}, Q^* = Q_N = I_q^* ((\bar{V}_\alpha^+)^2 + (\bar{V}_\beta^+)^2)^{0.5}$ ), as well as the given normal rated current (i.e.  $I_N$ ). Two parameters ( $k_p$  and  $k_q$ ) should be properly selected. Since this parameter selection process is highly non-linear, an off-line calculated look-up-table (LUT) is utilized in this paper. The next stage corresponds to the current PI control process. At the end of the current control loop, the duty cycles are processed by the pulse width modulator to drive the switch  $u$ . In the following, four different operational modes are analyzed to discuss possible transient processes.

Control situation 1 (CS1): it presents a scenario with relatively low active power production, and the current set-point is fixed to the normal rated value (i.e.  $I_N$ ). For example, if the abnormal condition with the voltage imbalance occurs, CS1 acts as a power-dispatch scheme in which a more considerable amount of reactive power is expected to mitigate the voltage imbalance. Control situation 2 (CS2): it presents a scenario with high active power production. This case is realized to produce more active power by monotonically increasing the parameter  $k_p$ , and then it is easy to obtain a lower demand for the reactive power if the parameter tends to act as  $k_q \rightarrow 0$  (e.g.  $k_q = 0.3$ ). Control situation 3 (CS3): it presents a scenario with an intermediate power production. It is realized to produce an intermediate power between CS1 and CS2 in order to highlight the adjustable feature of the proposed control method. Control situation 4 (CS4): it presents a scenario which combines the best features of the above three cases. In CS4, it can be observed that, when the  $P_{dc}$  is close to the value in CS1, then CS4 set-point approaches to CS1 set-point. However, if the  $P_{dc}$  approximately equals to the value in CS2, the maximum variation of the CS2 set-point is reached. In other words, the CS4 accomplishes a transition to the CS2 strategy. In summary, an adjustable power dispatch is realized in CS4. Results of four different cases have been conducted by experimental tests: low-, large-, intermediate-, and synthesis-dispatch scenarios. Table 1 summarizes the results of the four tests.

**TABLE 1** The measured P(Watts) and Q(Vars) for the four CS

Situation	Adjust parameter	$\bar{p}^+ + \bar{p}^-$	$\bar{q}^+ + \bar{q}^-$
CS1	$\kappa_p = 0.2; \kappa_q = 0.9$	120	800
CS2	$\kappa_p = 0.2 \rightarrow 0.5 \rightarrow 0.8; \kappa_q = 0.3$	120 $\rightarrow$ 300 $\rightarrow$ 480	270
CS3	$\kappa_p = 0.7 \rightarrow 0.6 \rightarrow 0.5; \kappa_q = 0.6$	420 $\rightarrow$ 370 $\rightarrow$ 310	510
CS4	$\kappa_p = 0.9 \rightarrow 0.6 \rightarrow 0.3$ $\kappa_q = 0.2 \rightarrow 0.5 \rightarrow 0.8$	540 $\rightarrow$ 380 $\rightarrow$ 190	180 $\rightarrow$ 440 $\rightarrow$ 700

**FIGURE 7** Detailed experimental setup**TABLE 2** System parameters for the DVR experimental setup

DVR (exclude injected transformer)		Injected transformer of DVR	
Parameter	Value	Parameter	Value
PWM switching frequency	2 kHz	Power	4.5 kVA
Filter inductance	1.4 mH	Primary voltage	380 V
Filter capacitance	15 $\mu$ F	Secondary voltage	380 V
Vdc voltage	170 V	Magnetization resistance	200 p.u.
Load power	3 kW 0.83PF lag	Magnetization inductance	200 p.u.

## 4 | EXPERIMENTAL RESULTS

In this section, a set of experimental tests has been carried out to validate the theoretical analysis. The laboratory test setup mainly consists of a Chroma programmable ac source 61611, a Chroma programmable dc power supply 62100H-600, a Chroma programmable ac electronic load 63804, and two Danfoss FC 302 converters. The detailed experimental setup is shown in Figure 7. The control algorithm is implemented in dSPACE DS1202, and the system parameters are listed in Table 2.

The tests are conducted under the following procedure: First, before 0.1 s, the PCC voltage is roughly balanced. Then, one phase voltage sag of 0.5 p.u. including a phase jump of 25° occurs at the time  $t = 0.1$  s. Finally, the voltage sag has been completely removed at  $t = 0.4$  s.

### 4.1 | Maximum power dispatch to the AC network

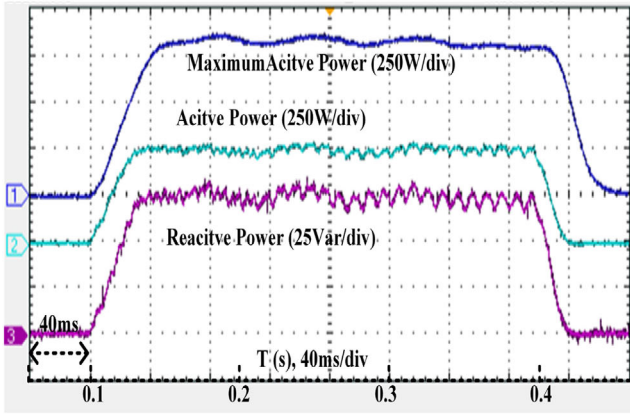
Appropriate power dispatch under the abnormal AC condition is an important issue for the DVR system. The deeper the voltage sag is, the higher the power requirements will be. In extreme cases, 100% of power dispatches are needed and the vector diagram for this condition is described in Figure 4. However, the effective injection of the active and reactive power is required so that the power dispatch can be achieved to support the load voltage. At the same time, the excessive active power should be removed to avoid dc-link over voltage issue. Thus, protection operation should be activated, as shown in Figure 5. Assuming that the network needs a certain amount of reactive power or a particular power dispatch, it is necessary to inject a certain amount of active power according to the load demands. This situation will also be recognized as the extreme cases (100% of power dispatch) and the injected reference power and the control parameters should be selected intentionally.

Extreme case 1: maximizing the active power. The active power is  $P_{dc} = P^*$ , and the DVR system parameters can be set as:  $Q^* = 75\text{Var}$ ,  $\kappa_p = 0.9$ , and  $\kappa_q = 0.1$ , respectively. Then, the maximum value of active power can be calculated based on (22) to keep the normal rated current equal to  $I_N = 7.6\text{A}$ .

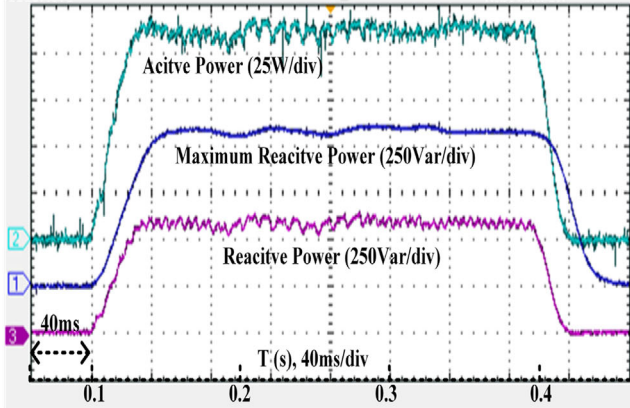
Extreme case 2: maximizing the reactive power. The reactive power is  $Q^*$ , and the DVR system parameters can be set as:  $P^* = 110\text{W}$ ,  $\kappa_p = 0.1$ , and  $\kappa_q = 0.8$ , respectively. Again, the maximum value of reactive power can be calculated based on (24) to keep the normal rated current equal to  $I_N = 7.6\text{A}$ .

The first experiment is conducted to evaluate the reference generators proposed in (16)–(19) based on Extreme case 1.  $P_{max}$  is increased from 0 to a maximum value of 850W as displayed in Figure 8a. It is worth of mentioning that the measured active power (i.e. 500 W) never increases up to  $P_{max}$  when the external reactive power demands  $Q^* = 75\text{Var}$ . The second experiment based on the Extreme case 2 indicates the maximum reactive power in Figure 8b considering  $P^* = 110\text{W}$ . Again, it can be observed that  $Q_{max}$  is increased from 0 to a maximum value of 880Var. However, the measured reactive power is 600Var that feeds the load voltage during the entire test. It can be seen that the load voltage profile based on Extreme case 1 is smoothly regulated when a voltage sag occurs, and it is also maintained at the desired level, as shown in Figure 8c. And thus, in the case of the maximum active or reactive power injection scenarios, it can be observed that the oscillation of both active or reactive power are negligible as desired due to the proposed control method.

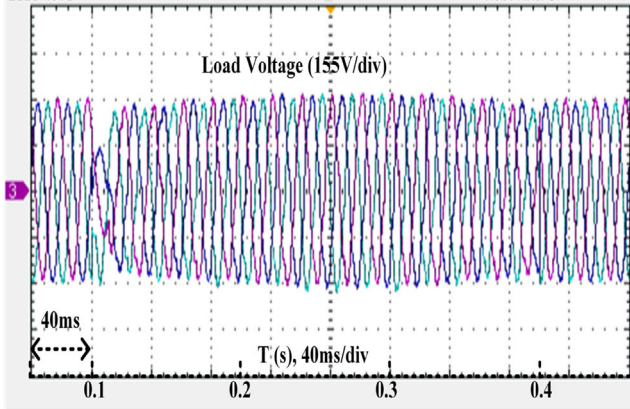




(a) Measured active power  $\bar{p}^+ + \bar{p}^-$ , reactive power  $\bar{q}^+ + \bar{q}^-$  and maximum power  $P_{max}$ .



(b) Measured active power  $\bar{p}^+ + \bar{p}^-$ , reactive power  $\bar{q}^+ + \bar{q}^-$  and maximum power  $Q_{max}$ .

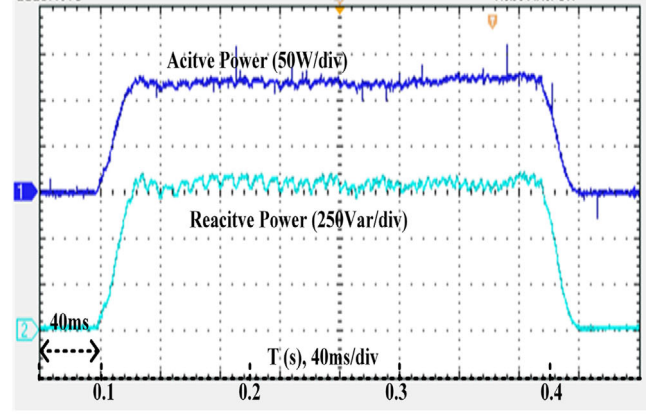


(c) Experimental load voltages

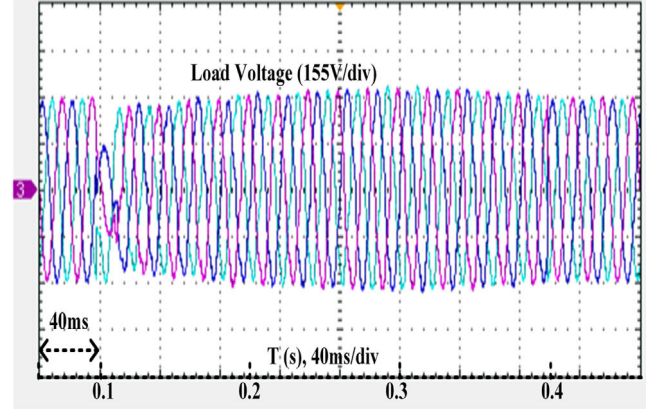
FIGURE 8 Experimental results for the maximum power injection scenario

## 4.2 | The performance of the flexible active and reactive power dispatch

A new group of experiments is conducted to estimate the voltage control situations mentioned in Section 3.2. In this case, the power dispatch scenarios shown in Table 1 are activated to



(a) Measured active power  $\bar{p}^+ + \bar{p}^-$  and reactive power  $\bar{q}^+ + \bar{q}^-$



(b) Experimental load voltages

FIGURE 9 Experimental results for CS1 scenario

provide variable values for the power setpoint and the control parameters ( $k_p$  and  $k_q$ ).

The performance of the proposed CS1 is clearly depicted in Figure 9. The measured active power is increased from 0 to a maximum value of 120 W, which is far away from  $P_{max}$ , while the measured value of the injected reactive power reaches almost 800Var, as shown in Figure 9a. The load voltage waveforms are presented in Figure 9b. For constant  $k_p$  and  $k_q$  values, the injected active power and reactive power can be independently regulated while maintaining the load voltage within the safe range during voltage sag.

Similar results are noticed in Figure 10 when CS2 is implemented. In this case, the measured value of the injected reactive power is constant (i.e. 270Var), while the measured active power is 120 W. The active power is increased to 300 W in the middle of Figure 10, and the final value of the measured active power is equal to 480 W at the top of Figure 10. The experimental results of CS3 is shown in Figure 11, it is interesting to note that the measured active power displayed at the top of Figure 11 equals to 420 W. Then the active power is reduced to 370 W at the middle of Figure 11. And the final value of the measured active power is equal to 310 W at the bottom of Figure 11. During the whole process the active power produced by DVR is below  $P_{max}$  while the measured reactive power is fixed at 510Var, as shown in Figure 11. In addition, the dynamic phenomenon for

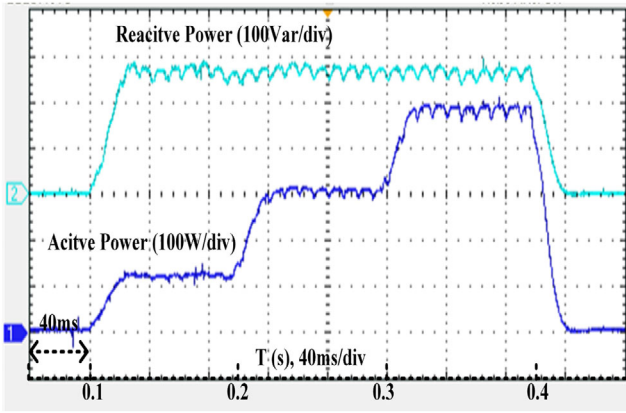


FIGURE 10 Experimental results for CS2 scenario

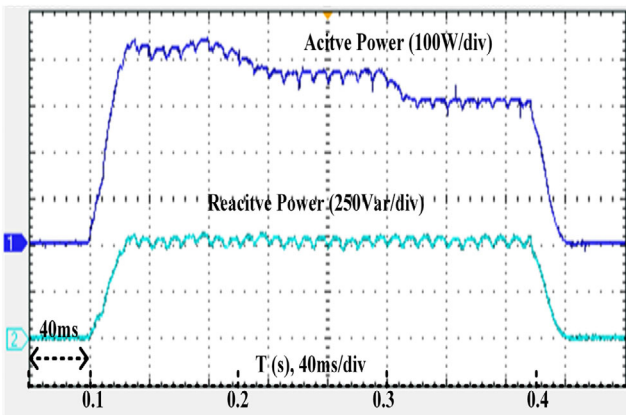
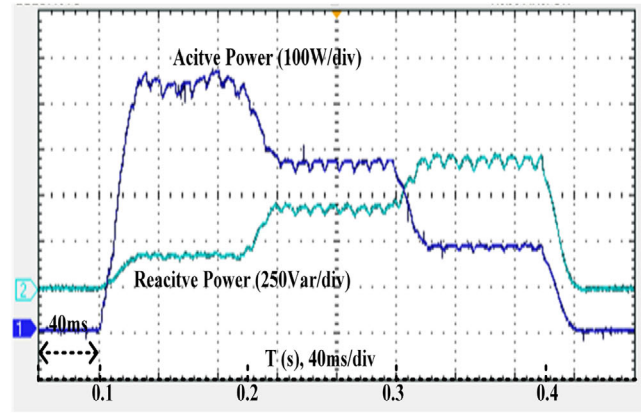


FIGURE 11 Experimental results for CS3 scenario

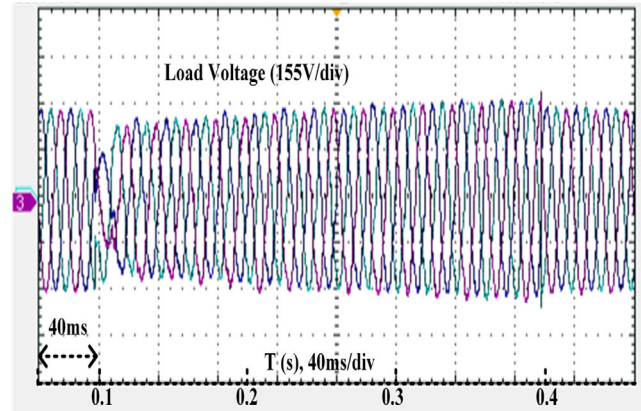
the load voltage during the CS2 and CS3 can also be obtained and are quite similar to the Figure 9b.

Experimental results implementing the presented control situation of CS4 is shown in Figure 12. The measured active power is increased from 0 W to a maximum value of 540 W at the top of the upper curve in Figure 12a. Then this value is decreased to 380 W in the middle of the upper curve in Figure 12a, and the final amount of the injected active power is equal to 190 W at the bottom of the upper curve in Figure 12a. Again, the measured value of the reactive power is 180Var at the bottom of the lower curve in Figure 12a, then this value is increased up to 440Var in the middle of the lower curve in Figure 12a. The final measured value of the reactive power is equal to 700Var at the top of the lower curve in Figure 12a. In this case, the load voltage is also depicted in Figure 12b.

For the scenarios of CS2-CS4 with the monotonic change of individual parameter  $k_p/k_q$  or both of them, the oscillation of both active or reactive power are suppressed within a small value by the proposed method. The control of active power and reactive power are decoupled with each other with respect to different value of  $k_p$  and  $k_q$ , which proves that the flexible power dispatch capability of the proposed control strategy. It can also be found that the variation of load voltage is quite small during the adjustable control of DVR output power. Therefore, for the



(a) Measured active power  $\bar{p}^+ + \bar{p}^-$  and reactive power  $\bar{q}^+ + \bar{q}^-$



(b) Experimental load voltages

FIGURE 12 Experimental results for CS4 scenario

proposed control scheme, the active and reactive power injection can be tuned as indicated by above scenarios to fulfill the needs of the specific loads. Excellent dynamic properties of the proposed control strategy can also be revealed in Figures 10–12, which provide smooth transitions between the operation scenarios.

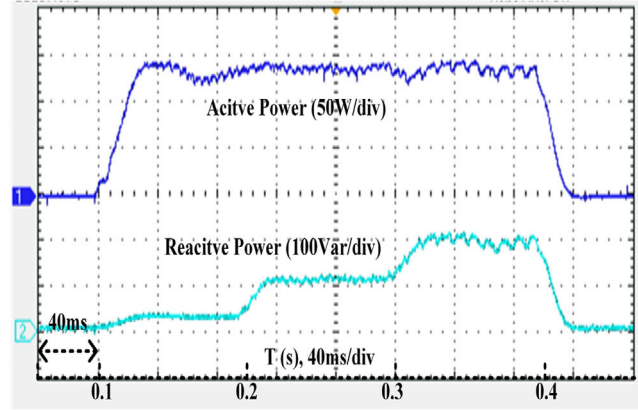
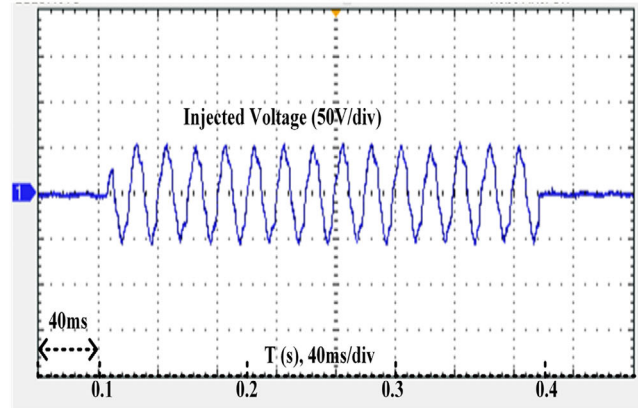
### 4.3 | Performance under different types of voltage sags

Another set of laboratory tests has been performed to illustrate the feasibility of the control scheme under different voltage sags. In this subsection, two different voltage sags have been programmed at the PCC voltage. The single phase (a-phase) voltage sag of 0.7p.u. is conducted in Test 1, in which the control parameter  $k_q$  is swept continuously ( $k_q = 0.1 \rightarrow 0.4 \rightarrow 0.7$ ) in the case of  $k_p = 0.5$ . In test 2, the two-phases voltage sag (b- and c-phase) of 0.3 p.u. is executed, in which the control parameter  $k_q$  is smoothly regulated ( $k_q = 0.1 \rightarrow 0.4 \rightarrow 0.7$ ) and  $k_p = 0.5$ . Other characteristic parameters are the same as the previously mentioned voltage sag. Table 3 summarizes the results for the two experimental tests.

Figure 13 shows the experimental results when the PCC voltage is perturbed by Test 1. In Figure 13a, the initial measured

**TABLE 3** Operating states during different sags

State	Test 1	Test 2
Sag depth (p.u.)	0.7	0.3
$\bar{p}^+ + \bar{p}^-$ (W)	140	300
$\bar{q}^+ + \bar{q}^-$ (VAr)	40 → 110 → 200	90 → 300 → 520

(a) Measured active power  $\bar{p}^+ + \bar{p}^-$  and reactive power  $\bar{q}^+ + \bar{q}^-$ 

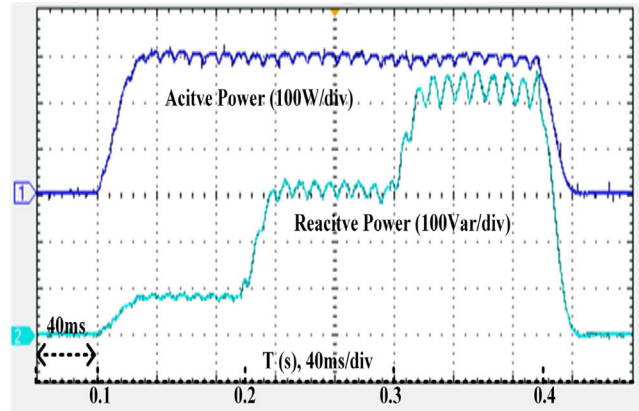
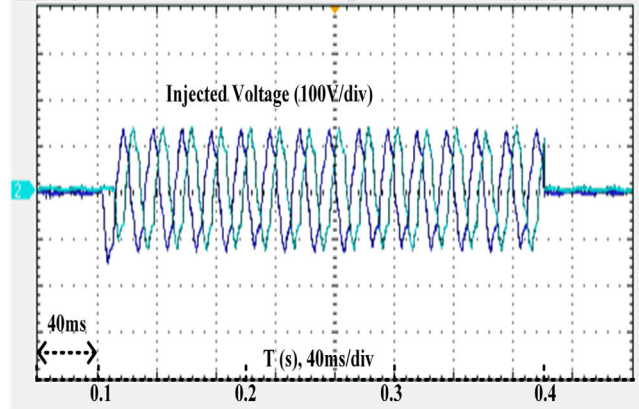
(b) Experimental output voltage

**FIGURE 13** Experimental results for the Test 1

total reactive power is 40Var, then this value is increased up to 110Var. The final amount of reactive power is equal to 200Var. However, the measured active power is roughly fixed at 140 W, as shown in Figure 13a. Then, the injected voltage is displayed in Figure 13b.

Figure 14 depicts the measured waveform when the PCC voltage is perturbed by Test 2. In Figure 14a, the initial measured total reactive power is almost 90Var, then this value is increased up to 300Va. The final amount of total reactive power is 520Var. However, the measured active power is roughly fixed at 300 W, as shown in Figure 14a. At the same time, the injected voltage is given in Figure 14b. The excellent dynamics performance of the given control schemes can be verified through the above experimental results.

One distinct advantage of the proposed control technique is a flexible selection of control parameters. Moreover, by utilizing

(a) Measured active power  $\bar{p}^+ + \bar{p}^-$  and reactive power  $\bar{q}^+ + \bar{q}^-$ 

(b) Experimental output voltages

**FIGURE 14** Experimental results for the Test 2

the variety of the two parameters, the reference current generators turn into a simple design to develop four suitable control situations. Besides, the proposed strategies provide excellent dynamic performance, which supports to obtain smooth transitions under power variations.

#### 4.4 | Discussion on the benefits of two control parameters

Depending on the previous experimental results, the benefits of two parameters for generating the current references in (16)–(19) during different voltage sags should be discussed. The critical function of the considered strategy is to achieve the zero oscillation of active and reactive power with a mechanism to maximize power delivery capacity. Table 4 provides a comparison of individual power injection. According to this table, six solutions are analyzed to explain the available selection of  $k_p$  and  $k_q$ , thus guaranteeing the flexible instantaneous power delivery.

The first solution is employed for implementing the constantly delivered power injection if two parameters are kept at constant values. The experimental results from the given CS1 can be utilized to verify the effectiveness of constant active and reactive power deliveries. When setting the control parameter  $k_p \rightarrow 1$  and  $k_q$  to be a constant, the second solution realizes the

**TABLE 4** The behavior of  $k_p$  and  $k_q$ 

$k_p, k_q \in [0, 1]$			Control		Objectives
No.	$(k_p,$	$k_q)$	P Control	Q Control	Smooth Transition
1	(Constant value,	Constant value)	P remains constant	Q remains constant	-
2	$(k_p \rightarrow 1$	Constant value)	$P \rightarrow P_{\max}$	Q remains constant	Only P
3	$(k_p \rightarrow 0$	Constant value)	$P \rightarrow 0$	Q remains constant	Only P
4	(Constant value,	$k_q \rightarrow 1)$	P remains constant	$Q \rightarrow Q_{\max}$	Only Q
5	(Constant value,	$k_q \rightarrow 0)$	P remains constant	$Q \rightarrow 0$	Only Q
6	$(k_p$ being monotonically changing,	$k_q$ being monotonically changing)	P flexible regulation	Q flexible regulation	P and Q

∴ Not Applicable

**TABLE 5** Comparison with previous strategies

No.	Injection power		Power control		Peak current limitation	Control Objectives		
	(P,	Q)	(P,	Q)	$I_{\max}$	Zero P oscillation	Zero Q Oscillation	$(P_{\max}, Q_{\max})$
[25]	(Yes,	No)	(Yes,	-)	No	Yes	-	(-, -)
[26]	(No	Yes)	(-,	Yes)	Yes	-	Yes	(-, -)
[27]	(Yes,	Yes)	(Yes,	Yes)	Yes	No	No	(Yes, Yes)
[28]	(Yes,	Yes)	(Yes,	Yes)	Yes	No	Yes	(No, Yes)
[29]	(Yes,	Yes)	(Yes,	Yes)	Yes	Yes	No	(Yes, No)
Proposed	(Yes,	Yes)	(Yes,	Yes)	-	Yes	Yes	(Yes, Yes)

∴ Not Applicable

monotonically increased active power regulation (i.e.  $P \rightarrow P_{\max}$ ) and constant reactive power delivery. The experimental results from the given CS2 can be utilized to verify the smooth transition of active power deliveries. By choosing the constant value of  $k_q$ , the third solution guarantees the monotonically decreased active power regulation (i.e.  $P \rightarrow 0$ ) and constant reactive power delivery. The experimental results from the given CS3 can also be utilized to verify the smooth transition of active power deliveries. Opposite to the second and third solutions,  $k_p$  is kept as a fixed value for the fourth and fifth solutions. The fourth solution achieves the monotonically increased reactive power regulation (i.e.  $Q \rightarrow Q_{\max}$ ) and constant active power delivery because of the parameter  $k_q \rightarrow 1$ . The experimental results from the given Test 1 can be utilized to verify the smooth transition of reactive power deliveries. By selecting the control parameter  $k_q \rightarrow 0$ , the fifth solution satisfies the monotonically decreased reactive power regulation (i.e.  $Q \rightarrow 0$ ) and constant active power delivery when setting the constant parameter of  $k_p$ . The experimental results from the given Test 2 can also be utilized to verify the smooth transition of reactive power deliveries. The same reason holds for the last solution by proper tuning of two parameters, and the flexible active and reactive power regulation can be realized at the same time. The experimental results from the given CS4 can be utilized to verify the smooth transition of active and reactive power deliveries.

The whole experimental setup contains the ac sag-source supply, DVR, dSPACE DS1202 and the load. A long transmission line is not included. Three types of ac sag-source with different grid-impedance ( $R/X$  ratio) are used to emulate the line impedance. The dynamic response of the presented four control situation can be described by using two control parameters.

For the voltage sag in a stiff grid (i.e. the higher value of  $R/X$  ratio), the maximum injection of active power can be achieved to raise the RMS voltage in each phase at the load side by the monotonic increase of control parameter  $k_p$ . The behavior of  $k_p$  and  $k_q$  in case 2 of Table 5 is utilized for this application. In contrary, when dealing with the voltage sag in a weak grid (i.e. the lower value of  $R/X$  ratio), the maximum injection of reactive power is required to restore the load voltage to the normal state. In this case, the control parameter  $k_q$  plays a vital role and the behavior of  $k_p$  and  $k_q$  in case 4 of Table 5 is applied.

The combination of active and reactive power injections is helpful to avoid the disconnection owing to overvoltage or undervoltage. The case 6 in Table 5 achieves the most flexible power injection by adaptively changing control parameters in accordance with the preset value distributions (e.g.  $k_p = 0.9 \rightarrow 0.6 \rightarrow 0.3$  and  $k_q = 0.2 \rightarrow 0.5 \rightarrow 0.8$ ). In this sense, the gradual transition from one power delivery level to another can be described accurately by these preset coefficient distributions, and it allows smooth transition during operational changes.

**TABLE 6** Comparison of dynamic response

Dynamic response	Proposed	Strategy				
		[25]	[26]	[27]	[28]	[29]
Time (ms)	15	13	10	20	25	12

In addition, it should be mentioned that the load voltage is slightly distorted once any type of voltage sags occurs. These slight undershoot responses are within one cycle (e.g. 15 ms), which is presented in two of three voltage phases during startup at  $t = 0.1$  s. The reason for this transient response comes mainly from three aspects: 1) the dead-time effect of the Danfoss 302 converter utilized in the experimental tests; 2) one fixed delay when the sequence extractors are used to detect the voltage components; 3) the abrupt parameter changes at  $t = 0.1, 0.2,$  and  $0.3$  s; Table 6 shows a comparison of different dynamic responses when implementing the proposed control strategy and conventional control strategies in [25–29]. Therefore, by proper selecting of two control parameters in (16)–(19), the appropriate operation mode can be decided once the equivalent impedance of ac sag-source (i.e.  $R/X$  ratio) and the characteristics of voltage sags at the PCC feeder are identified.

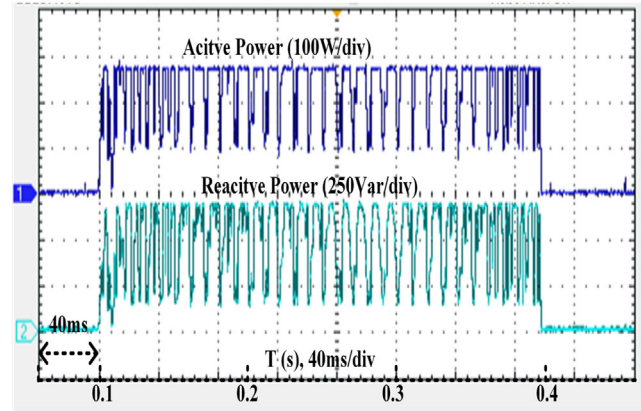
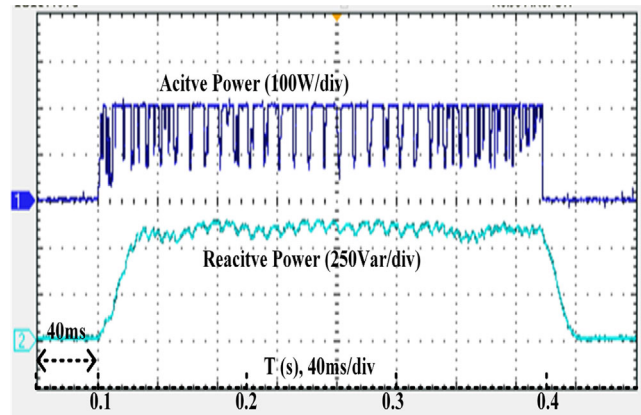
#### 4.5 | Comparison with the conventional strategies

The comparison results between the conventional strategies in [25–29] and the proposed method are listed in Table 5. The performance of the proposed control strategy is evaluated to support the PCC voltage with the flexible power dispatch during voltage sags. The different designs of two parameters for generating the current references in (16)–(19) are selected to obtain the control objectives in the last three columns of Table 5. For comparison, it is guaranteed that the conventional strategies also satisfy the two mathematical equations (i.e.  $i_{\alpha}^* = i_{\alpha(p)}^* + i_{\alpha(q)}^*$  and  $i_{\beta}^* = i_{\beta(p)}^* + i_{\beta(q)}^*$ ). According to Table 5, it can be found that only the proposed control strategy can achieve the zero oscillation of power injections and the maximum power delivery at the same time. In the following, the five control strategies are evaluated individually to reveal the effectiveness of the proposed controllers.

The control strategy [25] listed in Table 5 provides the flexible active power regulation that permits zero oscillation of active power. However, zero oscillation of reactive power and maximum power delivery are not applicable.

The control strategy [26] listed in Table 5 provides a reasonable reactive power injection that allows zero oscillation of reactive power. However, zero oscillation of active power and maximum power delivery are not applicable.

As to the control strategy [27] listed in Table 5, remarkable features of active and reactive power injections are displayed to maximize the power delivery capability of the voltage source converter and the maximum current is also smaller than the peak current limitation. The experimental results of strategy

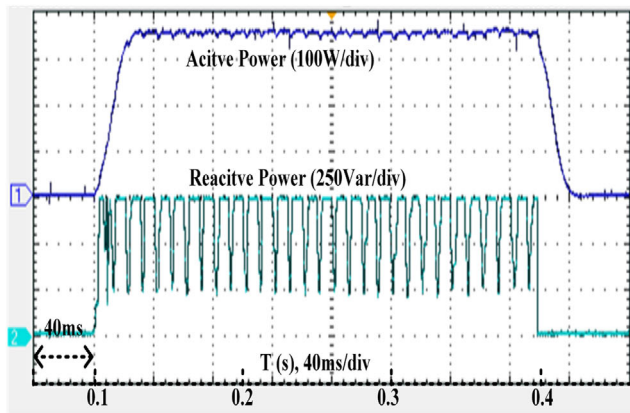
**FIGURE 15** Experimental results of the control strategy in [27]**FIGURE 16** Experimental results of the control strategy in [28]

[27] is displayed in Figure 15. Both of active power and reactive power suffer from large oscillation.

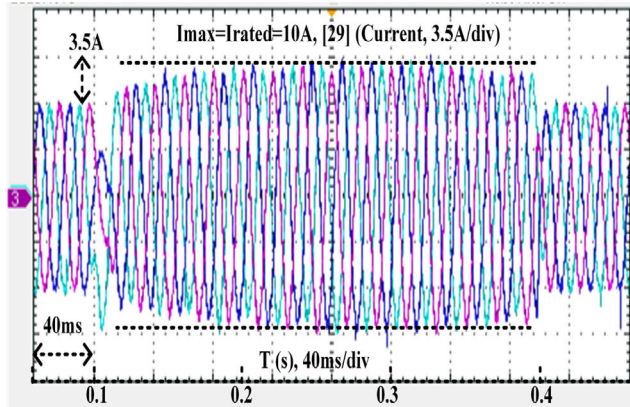
Based on the control strategy [28] listed in Table 5, the outstanding features of eliminating the reactive power oscillation can be achieved. It can be observed that the maximum reactive power delivery can be realized as high as 580Var, as shown in Figure 16.

With regards to the control strategy [29] listed in Table 5, a remarkable feature of the power injection that permits zero oscillation of the active power can be obtained. Figure 17a displays the measured active and reactive power injections (i.e. 350W and 500Var). The maximum current value of  $I_{\max}$ , can also meet the peak current limitation (i.e. 10A), as shown in Figure 17b. However, it suffers from large reactive power oscillation.

All considered control strategies except the first two strategies provide an outstanding feature that allows satisfying the process of the maximum active or reactive power injection. In summary, it is worth of mentioning that only the proposed control strategy can achieve zero power oscillation, maximum power delivery at the same time.



(a) Measured active power  $\bar{p}^+ + \bar{p}^-$  and reactive power  $\bar{q}^+ + \bar{q}^-$



(b) Experimental load currents

FIGURE 17 Experimental results of the control strategy in [29]

#### 4.6 | Computational load of the controller

Although the proposed current generators in (16)–(19), (22), and (24) may increase the inherent complexity of the given control schemes, the additional computational load can be ignored when the proposed algorithm is implemented in the dSPACE DS 1202 controller. The operational time of the whole algorithm is 11  $\mu$ s. This control strategy includes the A/D process, the voltage/current sequence detector, the current references, the current PI loop, and the PWM process. The total consumption of the operational time is increased by 9%, leading the idle period of 62% of the sampling time during voltage sags.

### 5 | CONCLUSIONS

A flexible power control scheme utilizing the elliptical trajectory has been presented in this paper. The mathematical relationship between the critical parameters and active and reactive power are studied. Based on the derived mathematical relationship, a reference generator is designed to accomplish two objectives: to keep the injected power within safety values and to compute the current references for a better uti-

lization of the DVR power capacity. The mathematical formulation proposed in this paper ensures the following: 1) the phase currents/power are controlled within safe range; 2) the control strategy is completely flexible to decide the active and reactive power references; and 3) the control method can improve unbalanced voltage sag operations. The mitigation of power oscillation, the smooth transition process of power control, and optimized power capacity are achieved simultaneously.

#### ACKNOWLEDGEMENTS

This work was supported by the China Postdoctoral Science Foundation under Project 2020M681093, and also supported by the Shenzhen Basic Research Project under Grant JCYJ20180306172056738.

#### ORCID

Frede Blaabjerg  <https://orcid.org/0000-0001-8311-7412>

#### REFERENCES

- Wang, J., et al.: A novel dual-dc-port dynamic voltage restorer with reduced-rating integrated dc-dc converter for wide-range voltage sag compensation. *IEEE Trans. Power Electron.* 34(8), 7437–7449 (2018)
- Pradhan, M., Mishra, M.K.: Dual  $p$ - $q$  theory based energy-optimized dynamic voltage restorer for power quality improvement in a distribution system. *IEEE Trans. Ind. Electron.* 66(4), 2946–2955 (2018)
- Jiang, F., et al.: Dual-functional dynamic voltage restorer to limit fault current. *IEEE Trans. Ind. Electron.* 66(7), 5300–5309 (2018)
- Torres, A.P., et al.: A two degrees of freedom resonant control scheme for voltage-sag compensation in dynamic voltage restorers. *IEEE Trans. Power Electron.* 33(6), 4852–4867 (2017)
- Priyavarthini, S., et al.: Pv-fed dvr for simultaneous real power injection and sag/swell mitigation in a wind farm. *IET Power Electron.* 11(14), 2385–2395 (2018)
- Shabestary, M.M., Mohamed, Y.A.R.I.: Asymmetrical ride-through and grid support in converter-interfaced dg units under unbalanced conditions. *IEEE Trans. Ind. Electron.* 66(2), 1130–1141 (2018)
- Guo, X., et al.: Flexible power regulation and current-limited control of the grid-connected inverter under unbalanced grid voltage faults. *IEEE Trans. Ind. Electron.* 64(9), 7425–7432 (2017)
- Rauf, A.M., Khadkikar, V.: An enhanced voltage sag compensation scheme for dynamic voltage restorer. *IEEE Trans. Ind. Electron.* 62(5), 2683–2692 (2014)
- Roiu, D., et al.: New stationary frame control scheme for three-phase pwm rectifiers under unbalanced voltage dips conditions. *IEEE Trans. Ind. Appl.* 46(1), 268–277 (2009)
- Meyer, C., et al.: Optimized control strategy for a medium-voltage dvr/theoretical investigations and experimental results. *IEEE Trans. Power Electron.* 23(6), 2746–2754 (2008)
- Choi, S., et al.: A generalized voltage compensation strategy for mitigating the impacts of voltage sags/swells. *IEEE Trans. Power Delivery* 20(3), 2289–2297 (2005)
- Li, P., et al.: A new voltage compensation philosophy for dynamic voltage restorer to mitigate voltage sags using three-phase voltage ellipse parameters. *IEEE Trans. Power Electron.* 33(2), 1154–1166 (2017)
- Li, P., et al.: New decentralized control scheme for a dynamic voltage restorer based on the elliptical trajectory compensation. *IEEE Trans. Ind. Electron.* 64(8), 6484–6495 (2017)
- Wang, F., et al.: Pliant active and reactive power control for grid-interactive converters under unbalanced voltage dips. *IEEE Trans. Power Electron.* 26(5), 1511–1521 (2010)

15. Valouch, V., et al.: Power control of grid-connected converters under unbalanced voltage conditions. *IEEE Trans. Ind. Electron.* 62(7), 4241–4248 (2014)
16. Tafti, H.D., et al.: Flexible control of photovoltaic grid-connected cascaded h-bridge converters during unbalanced voltage sags. *IEEE Trans. Ind. Electron.* 65(8), 6229–6238 (2017)
17. Chou, S.F., et al.: Average power balancing control of a statcom based on the cascaded h-bridge pwm converter with star configuration. In: 2013 IEEE Energy Conversion Congress and Exposition, pp. 970–977. IEEE, Piscataway (2013)
18. Zhang, Y., Qu, C.: Table-based direct power control for three-phase ac/dc converters under unbalanced grid voltages. *IEEE Trans. Power Electron.* 30(12), 7090–7099 (2015)
19. Zhang, Y., Qu, C.: Direct power control of a pulse width modulation rectifier using space vector modulation under unbalanced grid voltages. *IEEE Trans. Power Electron.* 30(10), 5892–5901 (2014)
20. Sosa, J.L., et al.: Control strategy to maximize the power capability of pv three-phase inverters during voltage sags. *IEEE Trans. Power Electron.* 31(4), 3314–3323 (2015)
21. Garnica López, M.A., et al.: Control strategy for grid-connected three-phase inverters during voltage sags to meet grid codes and to maximize power delivery capability. *IEEE Trans. Power Electron.* 33(11), 9360–9374 (2018)
22. Naidu, T.A., et al.: Multiobjective dynamic voltage restorer with modified ep11 control and optimized pi-controller gains. *IEEE Trans. Power Electron.* 34(3), 2181–2192 (2019)
23. Castilla, M., et al.: Voltage support control strategies for static synchronous compensators under unbalanced voltage sags. *IEEE Trans. Ind. Electron.* 61(2), 808–820 (2013)
24. Camacho, A., et al.: Reactive power control for distributed generation power plants to comply with voltage limits during grid faults. *IEEE Trans. Power Electron.* 29(11), 6224–6234 (2014)
25. Miret, J., et al.: Control scheme for photovoltaic three-phase inverters to minimize peak currents during unbalanced grid-voltage sags. *IEEE Trans. Power Electron.* 27(10), 4262–4271 (2012)
26. Castilla, M., et al.: Grid-fault control scheme for three-phase photovoltaic inverters with adjustable power quality characteristics. *IEEE Trans. Power Electron.* 25(12), 2930–2940 (2010)
27. Camacho, A., et al.: Flexible voltage support control for three-phase distributed generation inverters under grid fault. *IEEE Trans. Ind. Electron.* 60(4), 1429–1441 (2013)
28. Guo, X., et al.: Flexible power regulation and current-limited control of the grid-connected inverter under unbalanced grid voltage faults. *IEEE Trans. Ind. Electron.* 64(9), 7425–7432 (2017)
29. Camacho, A., et al.: Active and reactive power strategies with peak current limitation for distributed generation inverters during unbalanced grid faults. *IEEE Trans. Ind. Electron.* 62(3), 1515–1525 (2014)

**How to cite this article:** Li, P., Wang, Y., Wang, C., Pan, X., Lu, J., Li, X., Blaabjerg, F.: Flexible power control strategy for elliptical trajectory based dynamic voltage restorer during voltage sags. *IET Renew. Power Gener.* 15, 2904–2917 (2021).  
<https://doi.org/10.1049/rpg2.12222>